ChemPubSoc Europe

DOI: 10.1002/batt.201900020

BATTERIES & SUPERCAPS Communications

In situ Synthesis of a Bismuth Layer on a Sodium Metal Anode for Fast Interfacial Transport in Sodium-Oxygen Batteries

Mingyue Ma,[a] Yong Lu,[a] Zhenhua Yan,[a] and Jun Chen*[a]

Dedicated to the 100th Anniversary of Nankai University

Na metal has shown great promise as anode material for Na-based batteries due to its high theoretical capacity, low potential, high abundance, and low cost. However, the uneven solid electrolyte interphase layer formed on the Na anode surface caused by side reactions with the electrolyte and serious corrosion will lead to dendrite formation and safety issues. Here we report a stable Na anode by coating a Bi layer, which is formed in situ through simple ion-exchange. The compact Bi layer can effectively prevent Na reacting with the electrolyte and suppress the formation of dendrites. The Na/Bi anode exhibits high exchange current densities and fast charge-transfer kinetics. As a result, the overpotential of the symmetric cells using this Na/Bi electrode does not increase obviously after cycling for 1000 h at a current density of 0.5 mA cm^{-2}. Moreover, the Na–O_2 batteries with Na/Bi anode can run for 50 cycles. The presented surface coating approach provides a new strategy to protect Na anodes in Na-based batteries.

Na-based battery systems are considered as promising alternative candidates for large-scale energy storage owing to the high abundance and low cost of Na resources.[1] Among the anodes for Na battery systems, Na metal shows the lowest potential (−2.714 V *vs.* SHE) and the highest theoretical specific capacity (1165 mA h g^{-1}).[2] Furthermore, Na metal anode can be directly used for the high-energy-density battery systems such as Na–S batteries,[3] Na–CO_2 batteries,[4] and Na–O_2 batteries.[5] However, Na metal anode is plagued by many problems because of its intrinsic active chemical property. As a result of the reaction between organic solvent-based electrolyte and Na, unstable solid electrolyte interphase (SEI) would be formed during repeated charge/discharge cycles (Figure 1a). The reformation of SEI and uncontrolled Na dendrites can easily penetrate the separator and accelerate the loss of electrolyte and Na, resulting in short circuit of the batteries and safety accident.[6] In particular, this problem will be more serious under O_2 atmosphere because O_2 shows a stronger affinity for Na anode.[7]

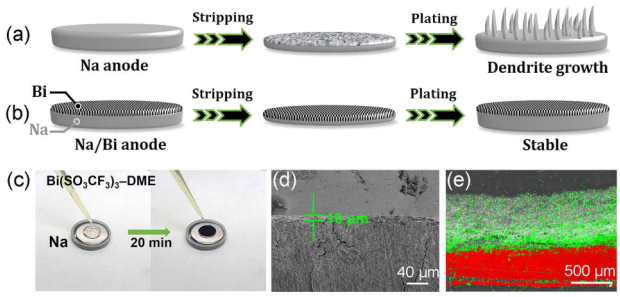

Figure 1. Na deposition models on a) Na and b) Na/Bi composite anode. c) Photographs of the synthetic processes of Na/Bi anode. d) Cross-sectional SEM image of the Na/Bi anode. e) EDS mappings of Bi (green) and Na (red).

Ether-based electrolyte is considered as one of the best systems for high-energy Na batteries due to the formation of a uniform SEI.[8] However, Sun's group showed that this SEI cannot maintain its stability at high current densities.[9a] Therefore, a successful SEI is critical for the electrochemical performance of Na anode. The ideal SEI should exhibit good properties such as tight contact with the electrode, high uniformity, stable mechanical and electrochemical properties, and high interfacial conductivity during stripping/plating. Previous works have revealed that constructing artificial SEI membranes (e.g., atomic Al_2O_3 layer,[9] ultrathin grapheme films,[10] inorganic-organic composite layer[11] and ionic liquid[12]) on the surface of Na can effectively protect Na metal. But these methods are relatively complicated and expensive, limiting their further applications. Recent studies on Li metal anode found that coating can provide a stable interface for Li deposition and accelerate Li ion diffusion.[13] However, as far as we know, there are few researchers focused on forming uniform layer for Na metal anode. Therefore, it is necessary to develop a type of low-cost artificial SEI membrane which can solve the most serious problems of Na electrode.

Herein, we demonstrate that the formation of bismuth metal artificial layer can solve the most serious problems of Na electrodes. Specifically, we realized the in situ produced Bi layer on Na metal anode (named as Na/Bi) via a facile replacement reaction. The Na/Bi anode can be used directly for electrochemical performance testing without further treatment. The

[a] Dr. M. Ma, Dr. Y. Lu, Dr. Z. Yan, Prof. J. Chen
Key Laboratory of Advanced Energy Materials Chemistry (Ministry of Education)
Renewable Energy Conversion and Storage Center
College of Chemistry
Nankai University
Tianjin 300071, China
E-mail: chenabc@nankai.edu.cn

Supporting information for this article is available on the WWW under https://doi.org/10.1002/batt.201900020

composite anode shows significant advantages, including accelerating charge-transfer kinetics, lowering the charge-transfer, protecting the Na anode from parasitic reactions, resistance, and suppressing dendrite formation (Figure 1b). The symmetric cells and Na–O_2 batteries with Na/Bi composite anodes show non-dendrite and long-life cycling performance.

Figure 1c shows the schematic diagram of producing the Na/Bi composite anode. When 40 uL 10 mmol/L $Bi(SO_3CF_3)_3$-dimethyl ether (DME) solution was dropped on the surface of Na anode, the color of the Na surface turns black quickly. This change implies the formation of Bi on Na surface. The reaction between Na and Bi^{3+} is warranted by the lower redox potential of Na^+/Na (−2.714 V vs. SHE) than that of Bi^{3+}/Bi (0.308 V vs. SHE):

$$Bi(SO_3CF_3)_3 + 3Na \rightarrow Bi + 3Na(SO_3CF_3)$$

The thickness of Bi layer is about 10 μm as measured by cross sectional scanning electron microscopy (SEM, Figure 1d). Compared with the Na electrode (300 μm), the Bi coating is very thin. Energy dispersive spectroscopy (EDS) mapping of the Bi and Na shows a uniform distribution of Bi in the layer (Figure 1e). The phase of Bi-coated Na composite anode was analyzed using X-ray diffraction (XRD, Figure 2a). The presence of Bi and Na peaks demonstrates the formation of Bi metal via the replacement reaction between $Bi(SO_3CF_3)_3$ and Na.

The high-resolution transmission electron microscopy (HRTEM) image of Bi is shown in Figure 2b. The *d*-spacing is about 0.33 nm, which matches well with the (012) facet of Bi (JCPDS 1-688). We further characterized the obtained Na/Bi composite anode by X-ray photoelectron spectrometry (XPS). As shown in Figure 2c, the Bi 4f spectra show two fully split peaks at 159 and 165 eV, implying the presence of Bi metal.[14] The other elements spectra such as Na 1s, F 1s, and C 1s could also be clearly seen in Figure S1. The Na 1s spectrum at 1072.6 eV corresponds to Na_2CO_3. The F 1s spectrum shows one peak centered at 688.4 eV confirming the existence of C–F. The C 1s spectra show three peaks at 286, 284.6, and 289.2 eV, corresponding to the exsitence of C–O, C–C, and O–C=O (related to organic carbonates), respectively. Overall, these results demonstrate that uniform Bi nanofilm forms on the surface of Na after the replacement reaction. The morphology of Na/Bi composite anode was observed by SEM. Unlike the bare Na anode with smooth surface, the Na/Bi anode shows porous morphology (Figure 2d), which is favorable for electrolyte penetration and ion transfer.

To investigate the effect of the concentration of Bi^{3+} on the thickness and microstructure of Bi layer, we chose three concentrations of Bi^{3+} solution (2, 10, and 20 mmol L^{-1}) to prepare the Na/Bi composite anode. As shown in Figure S2, with the concentration increasing, the morphology of the Bi becomes more compact and uniform, and the thickness of Bi layer increases (Figure S3). The concentrations of $Bi(SO_3CF_3)_3$-DME can also affect the overpotential and electrochemical impedance spectrum (EIS) of symmetric cells with Na/Bi electrode. The composite anode prepared by 10 mM Bi $(SO_3CF_3)_3$-DME (40 μL) shows the best performance among those obtained by other concentrations tested. In particular, the symmetric cells with the best anode exhibit the lowest overpotential of 8 mV at a current density of 0.25 mA cm^{-2} and the lowest charge transfer resistance of 6 Ω (Figure S4,S5). Considering the uniformity, overpotential, and electrochemical impedance of Na/Bi anode, we finally selected the concentration of 10 mM solution for subsequent experiments.

To demonstrate the interaction between Na ions and Na/Bi composite anode at the macroscopic scale, the contact angle test was conducted by dropping the electrolyte (1.0 mol L^{-1} $NaSO_3CF_3$ dissolved in diglyme (G2), 5 uL) vertically onto the Na and Na/Bi anodes (10 mm in diameter). As shown in Figure 3a,

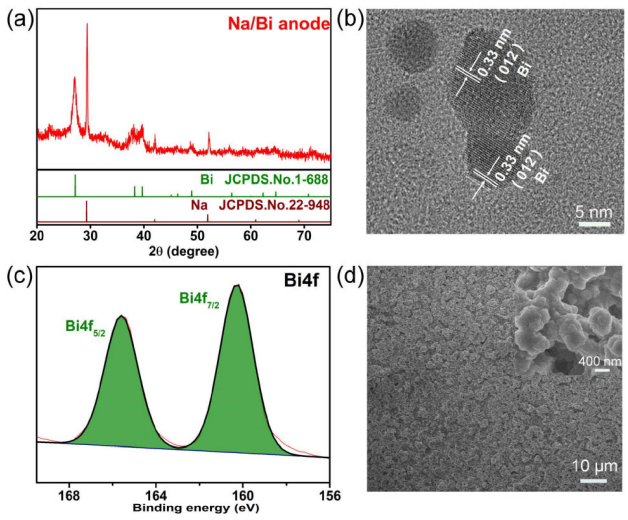

Figure 2. a) XRD pattern of the Na/Bi composite anode prepared by 10 mmol L^{-1} $Bi(SO_3CF_3)_3$-DME electrolyte. b) HRTEM image of the Na/Bi. c) Bi 4f XPS spectra of Na/Bi anode. d) SEM image of the Na/Bi composite anode. Inset: corresponding high-magnification SEM image.

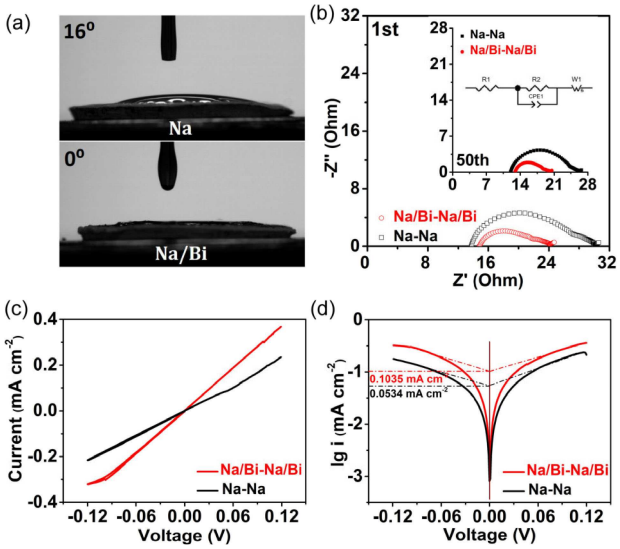

Figure 3. a) Contact angles of $NaSO_3CF_3$-G2 electrolyte on the Na anode and Na/Bi composite anode. b) EIS plots of Na and Na/Bi symmetric cells. c) CV curves at a can rate of 1 mV s^{-1} and d) Tafel plots of symmetric cells with Na/Bi composite anode and Na anode.

the contact angle of electrolyte droplet on the Na surface is 16°, indicating the moderate hydrophilicity of Na foil. Na/Bi anode exhibits a better hydrophilicity with a contact angle of about 0°, implying that electrolyte droplets can completely and rapidly penetrate into the Na/Bi anode networks. This difference can be ascribed to the different morphologies of the Na/Bi anode and the Na anode. The enhanced affinity of Bi layer with electrolyte decreases the concentration gradient of Na ion near the Na surface.[15]

The charge transport at Na/Bi electrode/electrolyte interphase can be deduced from impedance spectroscopy. Compared with the Na anode, Na/Bi composite anode shows a lower charge transfer resistance (6.5 vs. 15 Ω, Figure 3b), demonstrating that the formation of Bi layer promotes the transport of ions. The corresponding Bode plots of Na/Bi and Na symmetric cells after 1st and 50th cycle were shown in Figure S6. Moreover, the charge transfer resistance of the Na/Bi composite anode kept smaller than that of the Na electrode during the continuous cycles. To further study the electrochemical performance of Na/Bi composite anode, we conducted the cyclic voltammetry (CV) of the symmetric cells with the same size electrodes (Figure 3c). In the CV curves, the most significant feature between Na/Na cells and Na/Bi–Na/Bi cells is the difference of drastic slope. The Tafel plots were in turn obtained from CV for symmetric Na cells (Figure 3d). The results show that the exchange current for Na plating/stripping in Na/Bi anode ($I_0 = 0.1035$ mA cm^{-2}) is double higher than that of the pristine Na anode ($I_0 = 0.0534$ mA cm^{-2}), implying the charge transfer kinetics of Na/Bi anode is faster than that of the Na anode. The results demonstrate that the Bi artificial SEI membrane on sodium could accelerate charge transfer.

The macroscopic morphological evolution during deposition depend on the initial nucleation process and interfacial ion mobility. We observed the morphological evolution during sodium deposition on longer time scales by in-situ optical microscopy (sketch map in Figure S7). We use Na/Bi (or Na) as working electrode and Na/Bi (or Na) as the counter electrode, filling the center tube with electrolyte. Under a current density of 2 mA cm^{-2}, morphological changes of the electrode were recorded at equal time intervals up to 1 hour (2 mA h cm^{-2}), as shown in Figure 4a. Before deposition, the surfaces of both electrodes were smooth. After depositing for 60 min, the morphology of bare Na electrode was uneven and rough, implying the formation of Na dendrites and dead Na, leading to short circuit accident and low Coulombic efficiency. While for the Na/Bi electrode, the Na plating is smooth and compact, resulting in enhanced safety and Coulombic efficiency of the Na anode. Such difference can be more remarkable observed in the photograph of final deposition (Figure S8).

We further evaluate the electrochemical performance by using identical Na/Bi electrode with 1.0 mol L^{-1} $NaSO_3CF_3$-G2 solution as the electrolyte in 2032-type coin cell. Bare Na electrodes were also employed to be assembled in cells for comparison. These cells were discharged/charged at 0.5 mA cm^{-2} for 2 h (1 mA cm^{-2}, Figure 4b). Bare Na cells can run for 250 h and after that the voltage suddenly drops, suggesting that the short circuit happens. With regard to the

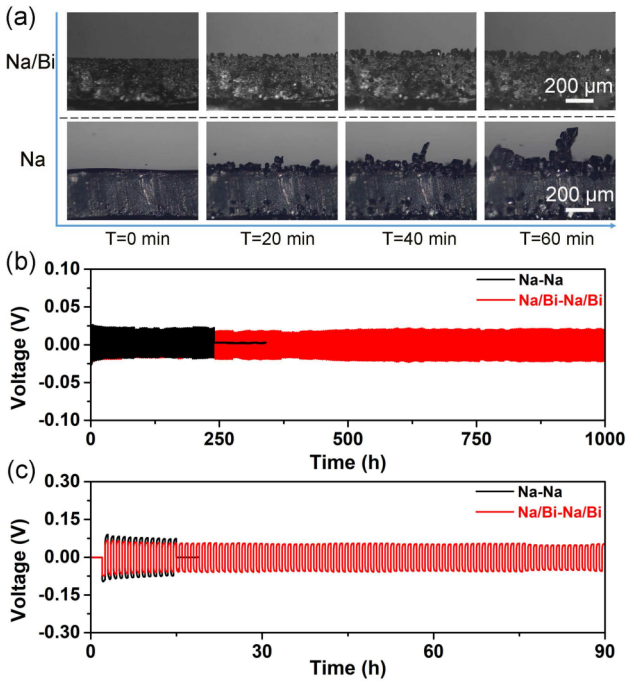

Figure 4. a) Operando optical microscopy images of the front surfaces of two electrodes (fresh composite anode or Na anode) in a transparent cell at a current density of 2 mA cm^{-2} for 1 h. Stripping/plating performance of symmetric cells with Na/Bi composite anode and bare Na metal anode at a current density of b) 0.5 mA cm^{-2} and c) 2 mA cm^{-2} for 1 mA h cm^{-2}.

Na/Bi cells, stable stripping/plating cycles can last for 1000 h. The cycling life of our cell with Bi layer outperforms all the other previous reports at a current density of 0.5 mA cm^{-2} (Table S1). The Na and Na/Bi anode after cycling were extracted and cleaned. Figure S9 shows the SEM images of Na and Na/Bi before and after cycling. It can be seen both anode surfaces before cycling are flat. After cycling, large amounts of dendrites appeared on the Na anode surface and caused cell short circuit. In contrast, there was no dendrite observed on the surface of Na/Bi, and the original appearance was basically maintained. Figure S10 shows the XPS spectra of Na/Bi composite anode surface after cycling, where the peaks of Bi metal still exist. The coating which is composed of fluorinated species and carbonate species remains integral during stripping and plating, indicating that the film is stable.

When the current density increases to 2 mA cm^{-2} (Figure 4c), the overpotential of bare Na exceeds 100 mV during cycling. The voltage suddenly drops to near 0 V after 13 cycles, indicating a short circuit in the battery owing to the formation of Na dendrites. In contrast, the Na/Bi composite anode shows lower initial overpotential (80 mV vs. Na^+/Na), and still maintains the overpotential of 75 mV (vs Na^+/Na) during cycling. Furthermore, higher current density is applied to show the superior performance of Na/Bi composite anode (Figure S11). Stable plating/stripping cycling for 150 cycles (equal to 70 h) with small overpotential can be obtained in the current density of 5 mA cm^{-2}, which is of great significance for these batteries with high energy density. When assembled into Na–Cu configuration batteries, the Na/Bi anode also shows

stable cycling performance. As shown in Figure S12, the Na/Bi–Cu batteries can run for 120 and 78 h at current densities of 1 and 2 mA cm^{-2}, respectively.

To further extend the practical application of the Na/Bi composite anode, we used it as anode in Na–O_2 batteries. The Na–O_2 batteries were assembled with 1.0 M $NaSO_3CF_3$ in G2 as the electrolyte, Super-P as the air cathode, and two pieces of glass fibre as the separator. The cycling performance of Na–O_2 batteries was evaluated at a large current density of 500 mA g^{-1} with a controlled discharge/charge capacity of 1000 mA h g^{-1}. The Na–O_2 batteries with Na anode only maintain ten cycles. The gap of the charge/discharge voltages increased from 320 to 500 mV and the discharge capacity decreases to 150 mA h g^{-1} (Figure 5a), meaning the failure of the batteries.

In contrast, the terminal voltage of the Na–O_2 batteries with Na/Bi composite anode does not decrease obviously after 50 cycles (Figure 5 b). Moreover, the battery achieves stable discharge capability of 1000 mA h g^{-1} during 50 cycles with high Coulombic efficiency of 96.3 % (Figure 5c), indicating good longterm cycling stability of Na/Bi–O_2 batteries. Furthermore, the discharge/charge profiles of Na/Bi–O_2 batteries at different rates (100, 200, 500, 1000 mA g^{-1}) with a controlled capacity of 1000 mA h g^{-1} are shown in Figure 5d. When the current densities increased from 100 to 1000 mA g^{-1}, the overpotential of batteries increased from 0.17 mV to 0.34 mV, implying the good high-rate performance of Na/Bi–O_2 batteries. SEM was further used to observe the change of the morphology of two different anodes after 10 cycles. As shown in Figure S13, mossy Na dendrites can be seen for Na anode. In contrast, the Na/Bi anode still maintains the original appearance. In addition, we found that the Na anode changed from metallic luster to silver after cycling, which may be related to the crossover of O_2. While the Na/Bi anode remained the original black (Figure S14). The XRD analysis further indicates the formation of NaOH on Na metal surface after cycling, but there was no obvious change for Na/Bi composite anode, demonstrating that the Bi layer on Na metal can prevent the crossover of O_2 (Figure S15).[7a] In addition, XRD and Raman were used to confirm the discharge products. As shown in Figure S16, S17, phase-pure NaO_2 was detected as the only product. Building a stable Bi layer can suppress electrolyte decomposition, O_2 crossover, improve Coulombic efficiency, and prevent dendrite formation in anode. Therefore, the Na–O_2 batteries with Na/Bi composite anode show enhanced cycling stability and improved discharge-charge ability when compared with that using bare Na anode.

In summary, we propose a feasible method to deposit Bi layer on the surface of Na metal anode via a replacement reaction. We find that the Na/Bi anode exhibits remarkably reduced interfacial impedance and high exchange current in diglyme-based electrolyte. The Na dendrites can be suppressed and long-term Na stripping/plating can be achieved without short circuit at different current densities. The symmetric Na/Bi cells can run for over 1000 h at a current density of 0.5 mA cm^{-2}. Furthermore, the Na–O_2 batteries with the Na/Bi composite anode also show improved cycling performance (50 cycles). This technique provides new route on protecting Na anode with high cycling stability and safety.

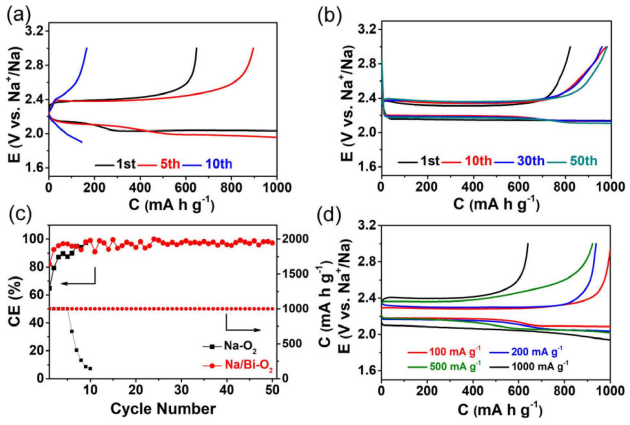

Figure 5. Discharge and charge profiles of Na–O_2 batteries with a) Na metal anode and b) Na/Bi anode. c) Coulombic efficiency and discharge capacity of Na/Bi–O_2 batteries and Na–O_2 batteries during charging/discharging processes at a current density of 500 mA g^{-1} (0.15 mA cm^{-2}). d) Rate performance of Na/Bi–O_2 batteries at different current rates (100, 200, 500, 1000 mA g^{-1}). The current densities and specific capacities were calculated based on the mass of Super-P in the cathode.

Acknowledgements

This work was supported by the National Programs for Nano-Key Project (2017YFA0206700), the National Natural Science Foundation of China (21835004), and 111 Project from the Ministry of Education of China (B12015).

Conflict of Interest

The authors declare no conflict of interest.

Keywords: bismuth protective film · dendrite prevention · interfacial transport · sodium metal anode · sodium-oxygen batteries

[1] a) H. Pan, Y.-S. Hu, L. Chen, *Energy Environ. Sci.* **2013**, *6*, 2338–2360. b) M. D. Slater, D. Kim, E. Lee, C. S. Johnson, *Adv. Funct. Mater.* **2013**, *23*, 947–958. c) S.-W. Kim, D.-H. Seo, X. Ma, G. Ceder, K. Kang, *Adv. Energy Mater.* **2012**, *2*, 710–721.d) Y. Xu, M. Zhou, Y. Lei, *Mater. Today* **2018**, *21*, 60–78. e) Y. Lu, Y. Lu, Z. Niu, J. Chen, *Adv. Energy Mater.* **2018**, *8*, 1702469. f) A. Jouhara, N. Dupré, A.-C. Gaillot, D. Guyomard, F. Dolhem, P. Poizot, *Nat. Commun.* **2018**, *9*, 4401.

[2] a) A. P. Cohn, N. Muralidharan, R. Carter, K. Share, C. L. Pint, *Nano Lett.* **2017**, *17*, 1296–1301. b) Y. Lu, L. Li, Q. Zhang, Z. Niu, J. Chen, *Joule* **2018**, *2*, 1747–1770.

[3] a) S. Xin, Y.-X. Yin, Y.-G. Guo, L.-J. Wan, *Adv. Mater.* **2014**, *26*, 1261–1265. b) S. Wei, S. Xu, A. Agrawral, S. Choudhury, Y. Lu, Z. Tu, L. Ma, L. A. Archer, *Nat. Commun.* **2016**, *7*, 11722. c) A. Manthiram, X. Yu, *Small.* **2015**, *11*, 2108–2114. d) Y.-X. Wang, J. Yang, W. Lai, S.-L. Chou, Q.-F. Gu, H. K. Liu, D. Zhao, S. X. Dou, *J. Am. Chem. Soc.* **2016**, *138*, 16576–16579.

[4] a) S. Xu, Y. Lu, H. Wang, H. D. Abruna, L. A. Archer, *J. Mater. Chem. A* **2014**, *2*, 17723–17729. b) Y. Lu, Y. Cai, Q. Zhang, L. Liu, Z. Niu, J. Chen, *Chem. Sci.* **2019**, *10*, 4306–4312. c) X. Hu, J. Sun, Z. Li, Q. Zhao, C. Chen, J. Chen, *Angew. Chem. Int. Ed.* **2016**, *55*, 6482–6486; *Angew. Chem.* **2016**, *128*, 6592–6596.

[5] a) P. Hartmann, C. L. Bender, M. Vracar, A. K. Dürr, A. Garsuch, J. Janek, P. Adelhelm, *Nat. Mater.* **2012**, *12*, 228–232. b) C. Xia, R. Fernandes, F. H. Cho, N. Sudhakar, B. Buonacorsi, S. Walker, M. Xu, J. Baugh, L. F. Nazar, *J. Am. Chem. Soc.* **2016**, *138*, 11219–11226. c) I. Landa-Medrano, R. Pinedo, X. Bi, I. Ruiz de Larramendi, L. Lezama, J. Janek, K. Amine, J. Lu, T. Rojo, *ACS Appl. Mater. Interfaces.* **2016**, *8*, 20120–20127. d) Z. E. M. Reeve, C. J. Franko, K. J. Harris, H. Yadegari, X. Sun, G. R. Goward, *J. Am. Chem. Soc.* **2017**, *139*, 595–598. e) K. Song, D. A. Agyeman, M. Park, J. Yang, Y.-M. Kang, *Adv. Mater.* **2017**, *29*, 1606572.

[6] a) H. Yadegari, Q. Sun, X. Sun, *Adv. Mater.* **2016**, *28*, 7065–7093. b) M. Han, C. Zhu, T. Ma, Z. Pan, Z. Tao, J. Chen, *Chem. Commun.* **2018**, *54*, 2381–2384.

[7] a) R. S. Assary, J. Lu, P. Du, X. Luo, X. Zhang, Y. Ren, L. A. Curtiss, K. Amine, *ChemSusChem* **2013**, *6*, 51–55. b) S. Wu, Y. Qiao, K. Jiang, Y. He, S. Guo, H. Zhou, *Adv. Funct. Mater.* **2018**, *28*, 1706374.

[8] a) Z. W. Seh, J. Sun, Y. Sun, Y. Cui, *ACS Cent. Sci.* **2015**, *1*, 449–455. b) P. Hartmann, C. L. Bender, M. Vracar, A. K. Durr, A. Garsuch, J. Janek, P. Adelhelm, *Nat. Mater.* **2013**, *12*, 228–232. c) L. Lutz, D. Alves Dalla Corte, M. Tang, E. Salager, M. Deschamps, A. Grimaud, L. Johnson, P. G. Bruce, J. M. Tarascon, *Chem. Mater.* **2017**, *29*, 6066–6075. d) J. Lee, Y. Lee, J. Lee, S.-M. Lee, J. H. Choi, H. Kim, M.-S. Kwon, K. Kang, K. T. Lee, N.-S. Choi, *ACS Appl. Mater. Interfaces.* **2017**, *9*, 3723–3732. e) R. Cao, K. Mishra, X. Li, J. Qian, M. Engelhard, M. Bowden, K. Han, K. Mueller, W. Henderson, J.-G. Zhang, *Nano Energy* **2016**, *30*, 825–830.

[9] a) Y. Zhao, L. V. Goncharova, A. Lushington, Q. Sun, H. Yadegari, B. Wang, W. Xiao, R. Li, X. Sun, *Adv. Mater.* **2017**, *29*, 1606663. b) W. Luo, C.-F. Lin, O. Zhao, M. Noked, Y. Zhang, G. W. Rubloff, L. Hu, *Adv. Energy Mater.* **2017**, *7*, 1601526.

[10] H. Wang, C. Wang, E. Matios, W. Li, *Nano Lett.* **2017**, *17*, 6808–6815.

[11] a) Y.-J. Kim, H. Lee, H. Noh, J. Lee, S. Kim, M.-H. Ryou, Y. M. Lee, H.-T. Kim, *ACS Appl. Mater. Interfaces.* **2017**, *9*, 6000–6006. b) Y. Zhao, L. V. Goncharova, Q. Zhang, P. Kaghazchi, Q. Sun, A. Lushington, B. Wang, R. Li, X. Sun, *Nano Lett.* **2017**, *17*, 5653–5659.

[12] S. Wei, S. Choudhury, J. Xu, P. Nath, Z. Tu, L. A. Archer, *Adv. Mater.* **2017**, *29*, 1605512.

[13] a) F. Chu, J. Hu, J. Tian, X. Zhou, Z. Li, C. Li, *ACS Appl. Mater. Interfaces.* **2018**, *10*, 12678–12689. b) S. Choudhury, Z. Tu, S. Stalin, D. Vu, K. Fawole, D. Gunceler, R. Sundararaman, L. A. Archer, *Angew. Chem. Int. Ed.* **2017**, *56*, 13070–13077. c) X. Liang, Q. Pang, I. R. Kochetkov, M. S. Sempere, H. Huang, X. Sun, L. F. Nazar, *Nat. Energy.* **2017**, *6*, 17119. d) Z. Tu, S. Choudhury, M. J. Zachman, S. Wei, K. Zhang, L. F. Kourkoutis, L. A. Archer, *Nat. Energy.* **2018**, *3*, 310–316. e) Q. Pang, X. Liang, I. R. Kochetkov, P. Hartmann, L. F. Nazar, *Angew. Chem. Int. Ed.* **2018**, *57*, 9795–9798.

[14] Q. Zhang, J. Mao, W. Pang, T. Zheng, V. Sencadas, Y. Chen, Y. Liu, Z. Guo, *Adv. Energy Mater.* **2018**, *8*, 1703288.

[15] X.-B. Cheng, T.-Z. Hou, R. Zhang, H.-J. Peng, C.-Z. Zhao, J.-Q. Huang, Q. Zhang, *Adv. Mater.* **2016**, *28*, 2888–2895.

Manuscript received: February 7, 2019
Revised manuscript received: April 4, 2019
Accepted manuscript online: April 11, 2019
Version of record online: April 25, 2019